minerals

MDPI

Article

Trace Elements in Chromian Spinels from Four Siberian Kimberlites

Marco Venier [1,*], Luca Ziberna [1], Francesco Princivalle [1], Maurizio Petrelli [2], Vanni Lughi [3], Alla Logvinova [4,5], Nikolay V. Sobolev [4,5], Gianluca Turco [6] and Davide Lenaz [1]

[1] Department of Mathematics and Geosciences, University of Trieste, 34128 Trieste, Italy
[2] Department of Physics and Geology, University of Perugia, 06123 Perugia, Italy
[3] Department of Engineering and Architecture, University of Trieste, 34127 Trieste, Italy
[4] Institute of Geology and Mineralogy, Siberian Branch of Russian Academy of Sciences, Novosibirsk 630090, Russia
[5] Department of Geology and Geophysics, Novosibirsk State University, 2, Pirogova, Novosibirsk 630090, Russia
[6] Department of Medical Sciences, University of Trieste, 34129 Trieste, Italy
* Correspondence: marco.venier@phd.units.it

Abstract: We analysed the major, minor and trace elements chemistry of forty-two Cr-spinels from four Siberian kimberlites. They showed a wide range in Mg# (Mg/(Mg + Fe^{2+}); 0.42–0.78) and Cr# (Cr/(Cr + Al); 0.32–0.92) and a common trend of increasing Cr# with decreasing Mg#. The major element classification schemes suggested that there were spinels deriving from a peridotitic source (Xen) and spinels crystallised from kimberlitic melts (Chr). Laser-Ablation Inductively Coupled Plasma Mass Spectrometry on both groups showed that the trace elements with the highest abundance were Mn (985–3390 ppm), Ni (531–3162 ppm), V (694–2510 ppm) and Zn (475–2230 ppm). Testing the effectiveness of trace elements in determining the source for Cr-spinels, we found out that Cr-spinels crystallised directly from a kimberlitic melt usually showed higher Mn, Ni, Sc and V concentrations with respect to those of peridotitic origin. In addition, using the available partitioning models, we found that the correlations between major elements and Ni, Co, Sc and Ga in the Xen group could be explained by subsolidus equilibration between spinel, olivine and clinopyroxene at 800–1000 °C, thus supporting a peridotitic source for this group. Finally, we calculated the composition of the possible melts in equilibrium with the Cr-spinels of the Chr group, using a selected set of partition coefficients. Calculated abundances of Cu, Ga and Zr were comparable to those of the kimberlite, while V was never close to the kimberlite composition. This simulation highlighted the need for new data on the trace elements partition coefficients between kimberlitic melts and Cr-spinel.

Keywords: trace elements; Cr-spinel; kimberlites; Siberia

Citation: Venier, M.; Ziberna, L.; Princivalle, F.; Petrelli, M.; Lughi, V.; Logvinova, A.; Sobolev, N.V.; Turco, G.; Lenaz, D. Trace Elements in Chromian Spinels from Four Siberian Kimberlites. *Minerals* **2022**, *12*, 1439. https://doi.org/10.3390/min12111439

Academic Editor: Fanus Viljoen

Received: 7 October 2022
Accepted: 11 November 2022
Published: 13 November 2022

1. Introduction

Spinels have been used as "petrogenetic indicators" since 1965 [1–3], thanks to their sensitivity to pressure–temperature conditions, bulk composition and oxidation state [2–8] and to their resistance to alteration during the serpentinisation of mantle peridotites [9]. This is true also for Cr-spinels from kimberlites, which are also commonly used as indicator minerals for diamond exploration [3,10]. Trace elements in such Cr-spinels are potential proxies for constraining their origin and the related petrogenetic processes. However, only a few studies so far have quantified the trace element budget in Cr-spinels from kimberlites, and either report only few analyses for a limited number of grains [11,12] or present large datasets limited to only few elements, such as Zn, Co and Ni [13]. In addition, a comprehensive characterisation of the whole spectrum of trace elements in

Cr-spinel from cratonic peridotites, which are common sources for Cr-spinel xenocrysts in kimberlites, is far from being complete [13–19]. This scarcity of data means that the distribution and partitioning of trace elements between Cr-spinels in kimberlites and their source assemblage cannot be well constrained. This can only be completed by acquiring new data on natural assemblages and by combining these data with the available partitioning models obtained through experimental and theoretical work.

The objectives of this work were (i) to quantify the trace element budget of Cr-spinels from kimberlites and its dependence on major element composition, (ii) to quantify the possible differences in trace element composition between Cr-spinels crystallised from kimberlitic melts from those that are fragments of peridotites, in order to implement the current criteria based on major elements variations, and (iii) to test whether the available experimental data could be used to model the partitioning between Cr-spinel and their source kimberlitic melts. This was completed by investigating a set of Cr-spinel grains selected from the mineral concentrates of four kimberlites from the Siberian craton, as a case study.

2. Geological Background

The Siberian craton extends over an area of ca. 4×10^6 km^2 and consists of Archean and Proterozoic blocks separated by suture zones [20]. It is divided into five major provinces, from west to east: Tunguska, Magan, Anabar, (the sum of Daldyn and Markha regions), Olenek (including Birekte and Hapchan regions) and Aldan-stanovoy. The Proterozoic Akitkan belt delimits the south margins of both Anabar and Magan provinces, extends for 1500 km and it is between 50 and 250 km wide [20]. The samples investigated in this study were from four kimberlite pipes: Aikhal and Komsomolskaya (Alakit field), located on the Anabar province, south-west of Udachnyj town, and Mir and International'naya (Mirny kimberlite field) from the Magan province, south of Mirnyj city. The eruption of these kimberlites is contemporary (367–345 Ma, $^{206}Pb/^{238}U$ ages; [21]) to the Devonian Viluy paleorift, located on the eastern part of the Akitkan belt [22]. All these kimberlites are Type I and diamondiferous [23]. The pipes are filled with breccia type olivine kimberlite with carbonate–olivine (or carbonate–serpentine if there were alterations) mesostasis.

3. Materials and Methods

We analysed forty-two spinels (four from Aikhal, seven from Komsomolskaya, fourteen from Mir, and nineteen from International'naya) selected under optical microscope from the heavy minerals concentrates of every pipe. These spinels were mounted on epoxy resin, ground to about half of their thickness and polished.

Back Scattering Electron (BSE) images and energy-dispersive X-ray spectroscopy (EDS) data were acquired with the Scanning Electron Microscope of the Department of Medicine, Surgery and Health Sciences in Trieste (Italy). Raman spectra were collected by a Renishaw InVia Spectrometer (objective 50× with 0.75 NA, 1200 lines/mm grating, 576 pixels CCD detector) at the Department of Engineering and Architecture in Trieste (Italy), in order to define the composition of inclusions in spinels. The excitation was a near-infrared diode laser at 785 nm excitation, delivering 16 mW at the sample surface, and a green diode laser at 514 nm, both focused on a spot of approximately 10 μm^2.

Chemical analyses were obtained by wavelength-dispersive X-ray spectroscopy (WDS) with a JEOL JXA-8200 electron microprobe at the Department of Earth Sciences "Ardito Desio", Milano (Italy). Analyses were performed under the following working conditions: 15 kV acceleration voltage, 5 nA beam current and 1 μm beam size. Peak and background counting times were 30 s and 10 s (for each side of the peak), respectively. Standards used were a combination of natural and synthetic minerals as well as pure metals: grossular for Al, pure Cr for Cr, olivine for Mg, ilmenite for Ti, fayalite for Fe, niccolite for Ni and rhodonite for Zn and Mn. Detection limits were in the range between 0.34 (for Al) and 320 (for Ni) ppm.

Laser Ablation-Ion Coupled Plasma-Mass Spectrometer (LA-ICP-MS) analyses were carried out using a New Wave UP213 (New Wave, UK) LA system coupled with a Thermo Electron X7 (Thermo Electron Corporation, Waltham, MA, USA) ICP-MS at the Department of Physics and Geology in Perugia (Italy). The LA system was a frequency quintupled Nd:YAG laser, whose fundamental wavelength of 1064 nm was converted into 213 nm. Helium was used as carrier gas and mixed with argon make-up gas before entering the ICP torch, permitting the maintenance of stable and optimum excitation conditions. Laser repetition rate and laser energy density were fixed to 10 Hz and 10 J/cm^2, respectively, during 120 s analyses (60 s for the gas blank and 60 s on the spinel). The analyses were conducted using a 15–30 μm beam diameter and the smallest diameter was used during the measurement of the thinnest spinels rim. Spinels were analysed for the following isotopes (the limit of detection expressed in ppm for every isotope is in brackets): ^{7}Li (1.11 ppm), ^{8}Be (0.25 ppm), ^{23}Na (25.23 ppm), ^{27}Al (2.65 ppm), ^{29}Si (1050 ppm), ^{39}K (5.62 ppm), ^{42}Ca (179.25 ppm), ^{45}Sc (0.66 ppm), ^{47}Ti (3.90 ppm), ^{51}V(0.40 ppm), ^{53}Cr (3.56 ppm), ^{55}Mn (2.63 ppm), ^{59}Co (0.53 ppm), ^{60}Ni (0.66 ppm), ^{65}Cu (0.93 ppm), ^{66}Zn (2.61 ppm), ^{71}Ga (0.09 ppm), ^{85}Rb (0.19 ppm), ^{88}Sr (0.02 ppm), ^{89}Y (0.01 ppm), ^{90}Zr (0.04 ppm), ^{93}Nb (0.02 ppm), ^{118}Sn (0.20 ppm), ^{133}Cs (0.07 pppm), ^{137}Ba (0.07 ppm), ^{139}La (0.01 ppm), ^{140}Ce (0.01 ppm), ^{141}Pr (0.01 ppm), ^{146}Nd (0.04 ppm), ^{147}Sm (0.06 ppm), ^{153}Eu (0.01 ppm), ^{157}Gd (0.05 ppm), ^{159}Tb (0.01 ppm), ^{163}Di (0.03 ppm), ^{165}Ho (0.01 ppm), ^{166}Er (0.02 ppm), ^{169}Tm (0.01 ppm), ^{173}Yb (0.04 ppm), ^{175}Lu (0.01 ppm), ^{178}Hf (0.02 ppm), ^{181}Ta (0.01 ppm), ^{208}Pb (0.06 ppm), ^{232}Th (0.01 ppm), ^{238}U (0.01 ppm). The analyses were calibrated against NIST SRM 610 [24] and USGS BCR2G glass reference materials, Mg values obtained by EMPA were used as the internal standard. Precision (expressed as relative standard deviation) was better than 10% for all the elements, while accuracy (expressed as relative deviation from the reference value) was always better than 11% with the only exception of Pb (15% ca.).

4. Results

4.1. Textures

The shapes of the grains were diverse, from a few well-faceted octahedral spinels (Figure 1c) to irregular and sub-rounded (Figure 1a,d). Most of them were subhedral (Figure 1f) to euhedral (Figure 1b). There were also some anhedral spinels interpreted as fragments of larger crystals. The average sizes did not exceed 0.6 mm, although some spinel grains may have reached 1 mm or more. BSE images showed that the grains were homogeneous. However, nineteen of the forty-four crystals were partially surrounded by thin rims with a spongy texture, formed by a variable number of micro-inclusions (arrows in Figure 1d). Some grains also contained inner isolated polymineralic inclusions (Figure 1e), some of which were partly or completely crystallised. EDS analyses suggested that some lamellar-shaped crystals within the polymineralic inclusions were K-bearing micas.

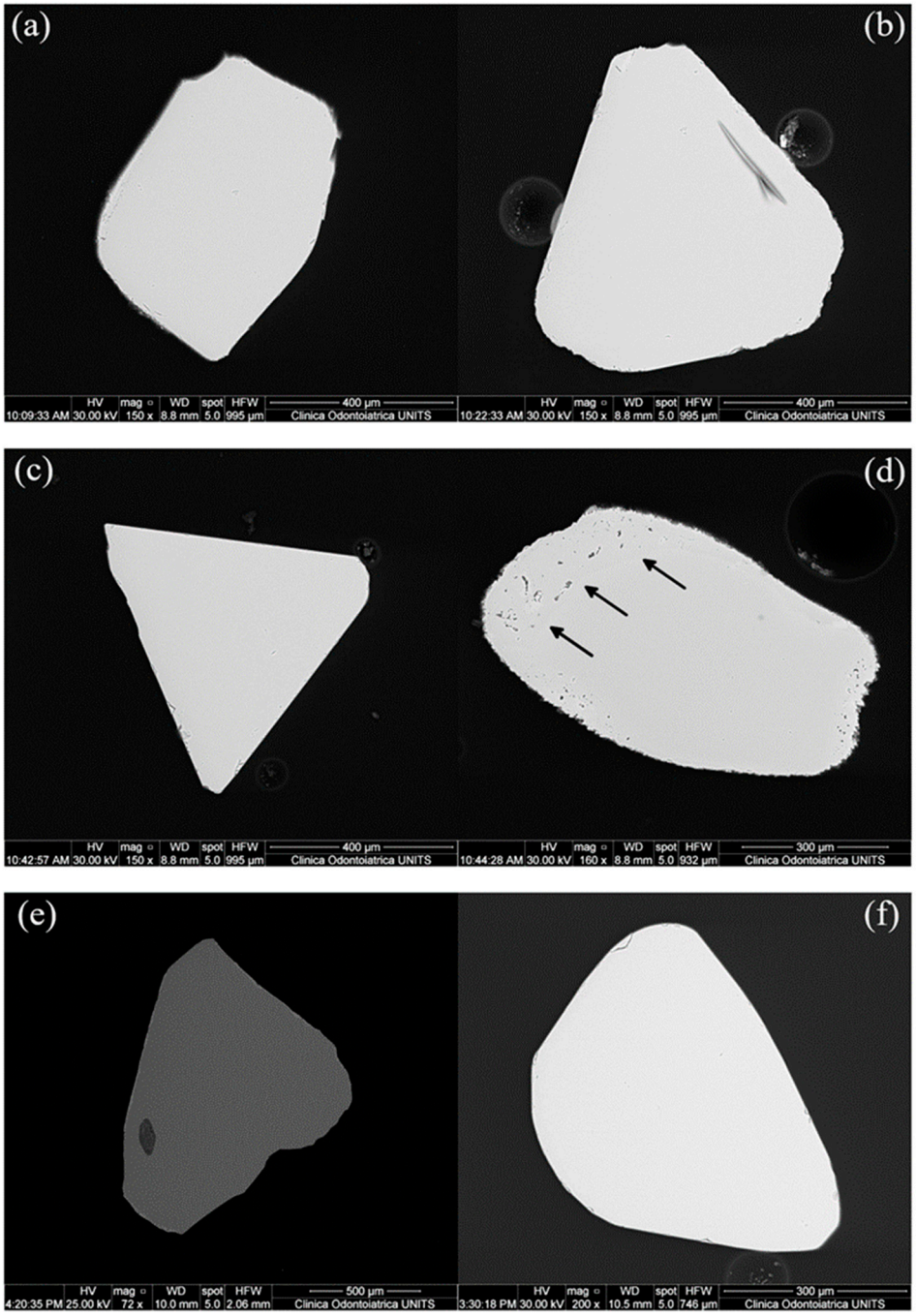

Figure 1. Backscattered electron images (BSE) of the Cr-spinels. (**a**) (M2_14) and (**b**) (M2_23) Cr-spinels from Mir pipe; (**c**) (M2_36) and (**d**) (M2_37) Cr-spinels from International 'naya, arrows indicate the rim; (**e**) (M1_09) Cr-spinel from Aikhal with a large polymineralic inclusion; (**f**) (M4_08) Cr-spinel from Komsomolskaya.

4.2. Major Element Chemistry and Classification

The results of EMPA analyses are tabulated in the Supplementary Data S1. The available Mössbauer and X-ray diffraction studies showed that Cr-spinels in diamonds and kimberlites were stoichiometric [25,26]. We therefore recalculated Fe^{2+} and Fe^{3+} by stoichiometry [27], which was assumed to be sufficiently accurate for the purpose of this study. Fe^{3+}# [Fe^{3+}/(Fe^{3+} + Al + Cr); atoms per formula unit, a.p.f.u., calculated on the base of four oxygens)] varied in the range 0.00–0.24, while Cr# [Cr/(Cr + Al)] varied in the range 0.32–

0.92. Mg# [Mg/(Mg + Fe^{2+})], which overall showed a negative correlation with Cr# (Figure 2), varied in the range 0.42–0.78. For most of the grains with spongy rims, Cr# and $Fe3^{+\#}$ were higher and Mg# was lower in the rims than in the cores (Figure 3a,b). TiO2 was systematically higher in the rims (0.26–9.50 wt%) than in the cores (<3.28 wt%), except for sample M01-10c, in which TiO_2 = 5.97 wt%. The texture and the high Ti content of the spongy rims suggested an origin by late reactions with the kimberlite magmas during or shortly before the eruption [28,29].

It is not straightforward to determine whether the cores of the grains represent fragments of an original peridotitic assemblage (i.e., xenocrysts) or the product of crystallisation from the kimberlite magma during its ascent through the lithosphere. As an estimate for their possible origin, here we adopted the classification scheme of Roeder and Schulze (2008) [30] (Figure 2) and found that 44% of the grains were classified as xenocrysts (Xen) and 56% as chromites crystallised from the kimberlite (Chr). This grouping is used in all the following discussions and figures.

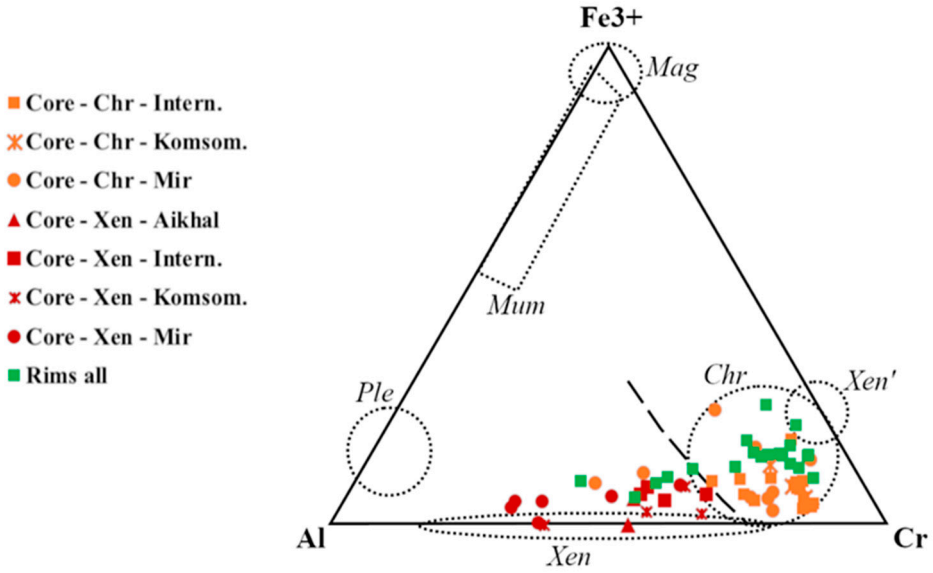

Figure 2. Compositional variations of Cr-spinel grains from this study shown in terms of Al-Fe^{3+}-Cr. Compositional fields are after Roeder and Schulze (2008) [30]. The dashed line was calculated in this work, see text.

Figure 3 shows a comparison between the two groups and some selected Cr-spinels from cratonic and non-cratonic peridotites. Figure 3a also shows that some of the samples were compatible with the "Trend 4" of Roeder and Schulze (2008) [30], suggested to represent xenocrysts that reacted with the kimberlitic magmas. No systematic relationships were found between the shape of the grains and their compositional classification.

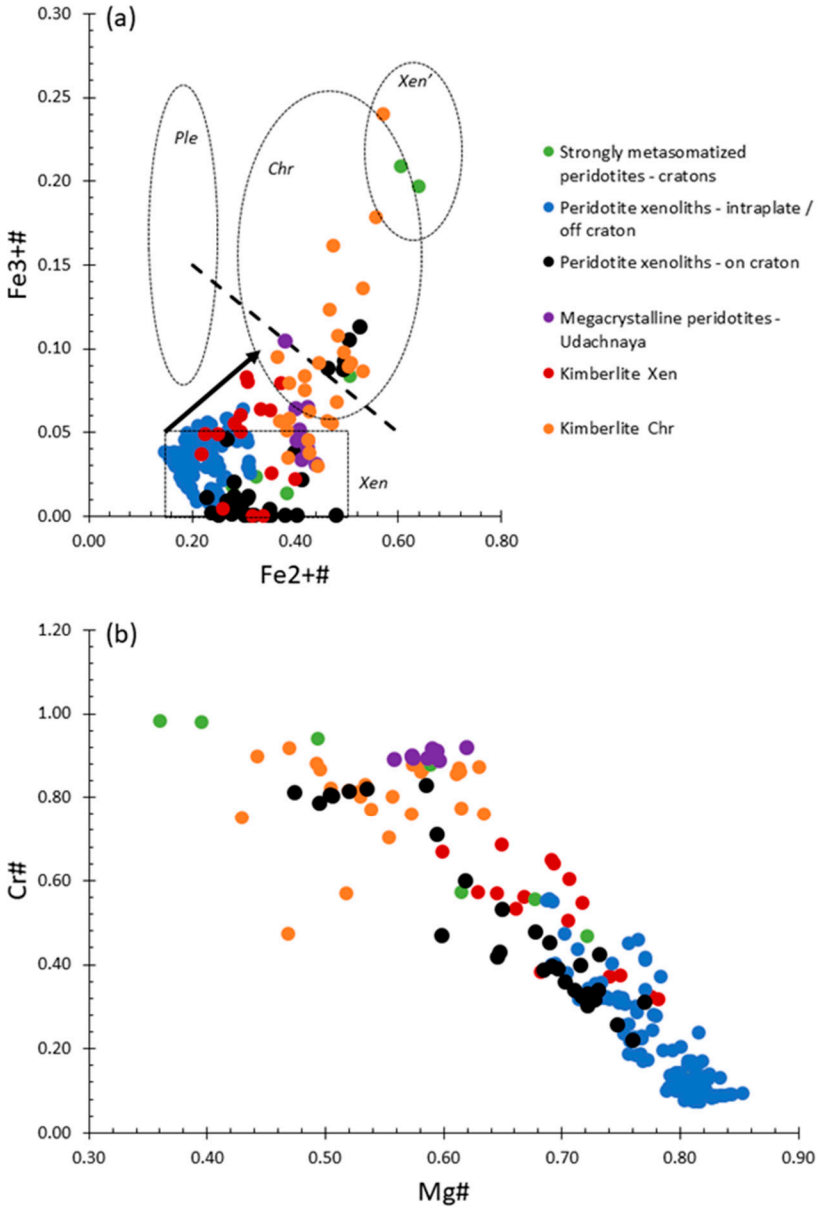

Figure 3. Compositional variations of Cr-spinel grains from this study shown in terms of: (**a**) $Fe^{2+}/Fe^{2+} + Mg$ (Fe^{2+}#) vs. $Fe^{3+}/Fe^{3+} + Cr + Al$ (Fe^{3+}#) and (**b**) Mg/Mg + Fe (Mg#) vs. Cr/Cr + Al (Cr#) projections. Compositional fields and trends (dashed shapes and black arrow) are after Roeder and Schulze (2008) [30]. The dashed line was calculated in this work and we classified as kimberlitic Chr the spinels either with Cr# > 0.75–0.667×Fe^{3+}# or Fe^{3+}# = 0.2–0.25 × Fe^{2+}#, while the remaining spinels wereclassified as Xen in kimberlite. Data for: strongly metasomatised peridotites from [19]; intraplate peridotite xenoliths from [15–18]; on-craton peridotite xenoliths from [31–33]; megacrystalline peridotites from [13].

4.3. Trace Element Chemistry

LA-ICP-MS analyses were performed on the homogeneous cores of all forty-two grains. The results are tabulated in the electronic supplement. Several tests were made to analyse the spongy rims, but the presence of closely-spaced inclusions (Figure 1d) and the relatively large, ablated volume (spot size = 15–30 μm, ablation depth > 10 μm) did not allow uncontaminated trace element data of Cr-spinel in the rims to be acquired.

The most abundant trace element was Mn, presenting a wide range between 985 and 3390 ppm, followed by Ni (531–3162 ppm), V (694–2510 ppm) and Zn (475–2230 ppm). All the other elements were always below 1000 ppm and included Co (201–444 ppm), Ga

(13.7–134.6 ppm), Cu (1.4–50.2 ppm), Sc (0.90–11.99 ppm), Zr (0.055–13.500 ppm), Nb (0.14–4.36 ppm), Sn (0.22–1.92 ppm) and Ta (0.01–0.54 ppm). Sr, Hf and Pb, which were in many cases (> 50% of the grains) below their detection limit, varied in the range 0.01–0.61 ppm, 0.02–0.30 ppm and 0.04–0.33 ppm, respectively. The other fifteen analysed elements (Rb, Y, Ba, La, Ce, Pr, Nd, Sm, Eu, Gd, Tb, Tm, Yb, Th, U) were below their detection limit for more than 85% of the grains. No systematic relationships were found between the trace element contents of the Cr-spinels and those of their host kimberlites (based on the compositions reported by [34]).

5. Discussion

In the following, we discuss the variations of trace elements in the Cr-spinels from this study and compare them with some available data of Cr-spinels in peridotites from other continental settings. For the sake of consistency, we only compare them with data obtained through LA-ICP-MS analyses.

5.1. Manganese

Manganese showed generally higher values in the Chr group (1753–3390 ppm) with respect to the Xen group (985–2093 ppm), the latter showing a well-defined negative correlation with Mg# (Figure 4a). Such a correlation was also observed in Cr-spinels in peridotites from other continental settings, which supports an origin of our Xen grains as fragments of peridotites, as suggested by the classification based on major elements. This correlation likely reflects the Fe^{2+}/Mn^{2+} subsolidus equilibria between olivine and spinel and the small variations of Mn contents in mantle peridotites (MnO = 0.13 ± 0.04 wt.% for peridotite xenoliths, based on the GEOROC database, http://georoc.mpch-mainz.gwdg.de accessed on 3 November 2021). These observations are consistent with Mn^{2+} being favoured in tetrahedrally-coordinated sites [35], in which an increase in the Fe^{2+}/Mg ratio corresponds to an increase in the average cation site ($^{IV}Fe^{2+}$ = 0.63 Å, ^{IV}Mg = 0.57 Å) and therefore to a major compatibility for the larger Mn cation ($^{IV}Mn^{2+}$ = 0.66. Å). The excellent correlation between Mn and Mg# excluded the possibility of Mn being in the trivalent state, in agreement with the few available experimental data on Mn partitioning [36].

Data for the Chr group were more scattered (Figure 4a), possibly because there were Cr-spinels crystallised from proto-kimberlitic melts at different stages of their evolution and therefore with variable Mn contents, or crystallised at different stages of kimberlite melt composition.

5.2. Zinc

Zinc did not show systematic differences between the Xen (475–2030 ppm) and Chr group (967–2230 ppm) but showed a perceivable negative correlation with Mg# (Figure 4b). As observed for Mn, this is consistent with Zn^{2+} favouring the tetrahedral site [14,35] occupied by Mg and Fe^{2+}. The large Zn variations at constant Mg# might be related either to temperature variations (cf. [37]), equilibration in compositionally diverse mantle peridotites (based on the GEOROC database, Zn in peridotite xenoliths varies between 12.9 and 160 ppm, with an average of 53 ± 18 ppm) or both. In addition, Zn in Cr-spinel has been found to vary also as a function of the sulphide content in the assemblage [14]. Zn is also known to be a moderately volatile element [36,38]. A role of COHS-bearing fluids, which are expected in sub-cratonic mantle environments related to kimberlite genesis, could therefore also be a controlling factor for the observed variability of Zn in both Xen and Chr spinels of this study. It is worth noting that Zn^{2+} and Co^{2+} in the tetrahedral coordination have a very similar ionic radius and consequently T-O distances (1.98 and 1.96 Å [39]; 1.96 Å for both [40]; 1.960 and 1.972 Å, [41]), which may explain the systematic correlations between these two elements in Cr-spinel from different host lithologies (this work, see Supplementary Figure S1 ; ophiolitic chromite [42–44]; magmatic and metamorphic chromite [44] Cr-spinel in mantle xenoliths [18]).

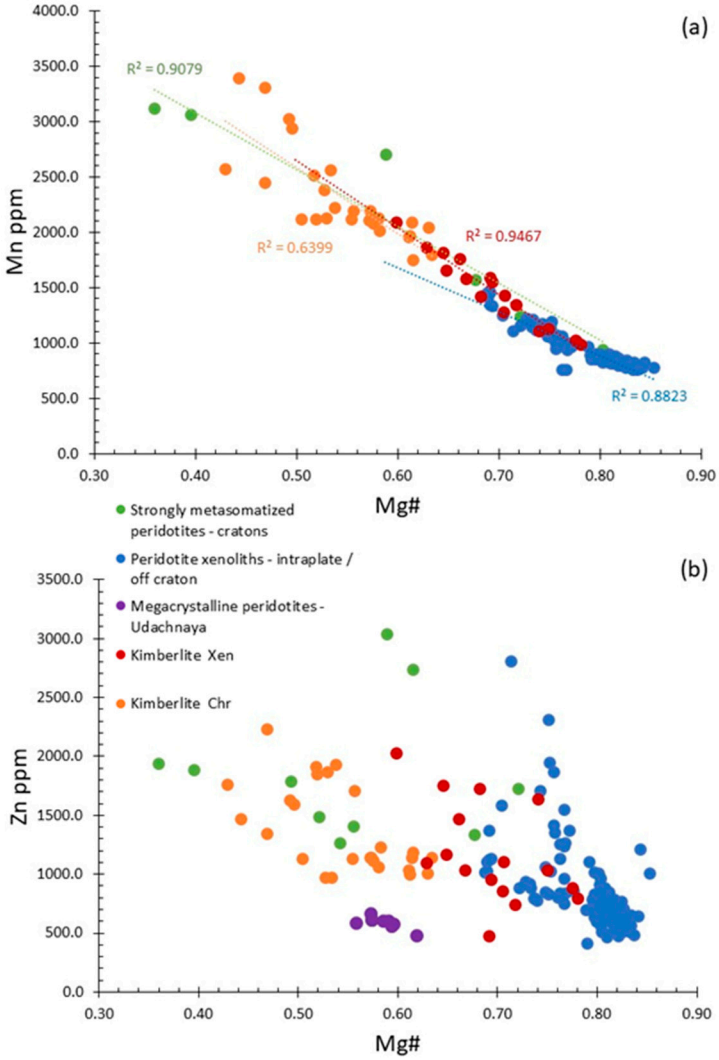

Figure 4. (**a**) Mg# vs. Mn and (**b**) Mg# vs. Zn for the Cr-spinels from this study. Data for peridotite xenoliths [15–18] are shown for comparison. Symbols and colors as in Figure 3.

5.3. Nickel, Co, Sc, Ga, V

Nickel in the Xen group (531–2236 ppm) was on average higher than in the Chr group (540–1520 ppm) and showed a crude progressive decrease with increasing Cr#, which is better defined by the xenolith suites from other continental settings (Figure 5a). This is consistent with Ni^{2+} having a high crystal field stabilization energy in the octahedral coordination [35,45], as already discussed by the authors of [14,46] for Cr-spinel from other geological settings.

Cobalt had no significant differences between the Chr and Xen groups (219.9–423.0 vs. 201.1–444.0 ppm, respectively). There was no correlation with Cr# and Mg#, similar to spinels in peridotites or included in diamond [13,18,47].

Scandium showed higher values in the Chr group (0.98–11.99 ppm) with respect to Xen spinels (0.90–5.31 ppm) and no correlation appeared with Mg#, nor with Cr#.

Gallium showed comparable ranges for the Xen and Chr group (13.7–91.2 vs. 14.9–134 ppm, respectively) and no apparent correlations with Cr# or Mg#. Paktunc and Cabri (1995) [14], who noted an inverse relationship between Ga and Cr/(Cr + Al + Fe^{3+}), suggested that Ga contents in Cr-spinel are controlled by the distribution of the trivalent cations. Dare et al. (2009) [48] suggested it should behave in a similar way to Fe^{3+} (as they

share the same ionic radius, i.e., 0.62 Å) and to Al. They also found that $Ga/Fe^{3+}\#$ ratios decreased during melt–rock reaction.

On average, V showed slightly lower values in the Xen group and a slightly positive correlation between V and Cr# and negative between V and Mg#. This correlation was more evident for samples from non-cratonic peridotites (Figure 5), as already shown by Lenaz et al. (2017) [18].

5.4. Trace Element Modelling for a Peridotitic Source

In order to constrain the source of the trace element variations in Cr-spinels from the Xen group, we used the partitioning models of Witt-Eickschen and O'Neill (2005) [15] to simulate the variations of Ni, Ga, Sc, V and Co as a function of Cr# for a hypothetical Cr-spinel in an equilibrated peridotitic assemblage. These models take into account the temperature and compositional dependence of the trace element partitioning between phases and were calibrated using a carefully selected set of natural mantle peridotites. Figure 5 shows the results of such models.

Nickel variation in Cr-spinel was calculated using the equation describing the Ni-Mg distribution coefficient between olivine and spinel [15], under the assumption that Ni variation in spinel is mainly controlled by equilibrium with olivine:

$$\boldsymbol{lnKD_{Ni/Mg}^{ol/sp} = ln\left(\frac{Ni^{ol}/Ni^{sp}}{Mg^{ol}/Mg^{sp}}\right) = \frac{1722Cr\#^{sp}}{T} - 1.118}$$

where Ni^{ol}, Ni^{sp}, Mg^{ol}, Mg^{sp} are the Ni and Mg contents in olivine and spinel, expressed either as a molar fraction or concentration (ppm or wt%) and T is temperature in K. The same approach was used for Co [15]. Figure 5 shows the calculated variations using $Mg^{ol}/Mg^{sp} = 3.4$, which corresponds to the average for peridotite xenoliths from the nearby Udachnaya kimberlite [31], with the assumption that our Cr-spinels from the Xen group were xenocrysts inherited from similar peridotites. We calculated four possible models by varying the temperature (800 °C and 1000 °C, which should bracket most of the temperatures obtained for spinel peridotites from the Siberian craton [31,49]) and the Ni and Co content of coexisting olivine (Ni^{ol}_{min} = 2780 ppm, Ni^{ol}_{max} = 3750 ppm, Co^{ol}_{min} = 128 ppm, Co^{ol}_{max} = 146 ppm; i.e., the lower and higher values measured in olivines from the same peridotite suite from Udachnaya; [31]). Although these assumptions may oversimplify the actual Ni and Co partitioning in peridotites, we note that this was only a semi-quantitative exercise to evaluate if the observed trace element variations in our Cr-spinels were compatible with equilibrium partitioning in mantle peridotites.

Figure 5a, b shows a good fit of the models within the Xen group. The calculated Ni content significantly decreased with increasing Cr# of spinel and slightly increased with increasing temperature from 800 °C to 1000 °C. Calculated Co contents showed a slight increase with increasing Cr# and a more significant effect of temperature (Figure 5b), with the Co contents decreasing as much as 90 ppm if the temperature was increased from 800 to 1000 °C, at a constant Cr#. Based on this model, Ni and Co variations shown by Xen Cr-spinels are compatible with equilibrium in a peridotitic assemblage at T = 800–1000 °C with Ni and Co contents in olivine in the range 2780–3750 ppm and 128–146 ppm, respectively. A small group of Cr-spinel grains with lower Ni (<1010 ppm) and higher Co contents (> 300 ppm; Figure 5a,b) possibly reflects assemblages with $Mg^{ol}/Mg^{sp} > 3.4$, which are less frequent but still present in the spinel and spinel–garnet peridotites from Udachnaya [31].

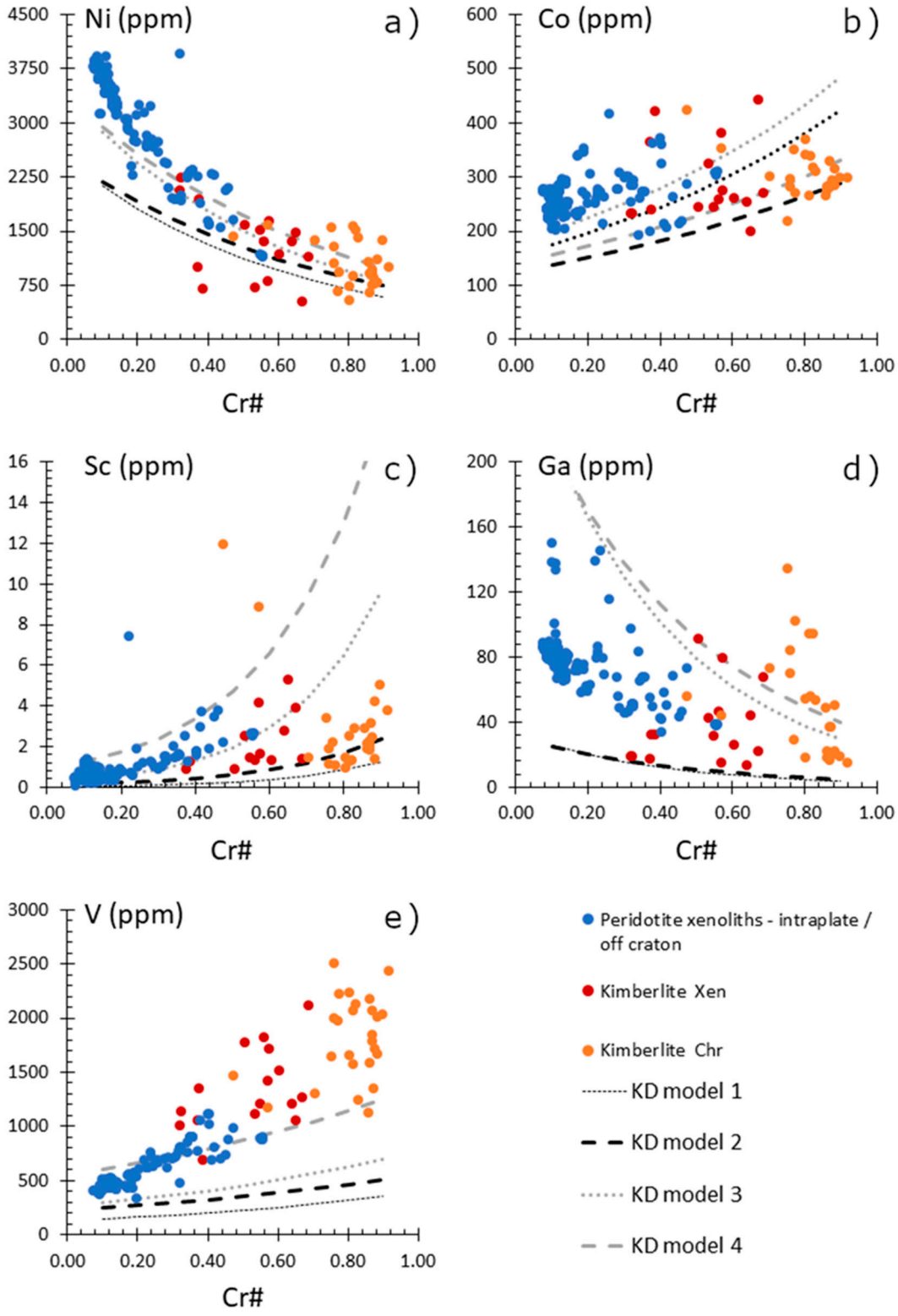

Figure 5. Cr# vs. Ni (**a**), Co (**b**), Sc (**c**), Ga (**d**) and V (**e**) for the Cr-spinels from this study and from peridotite xenoliths of continental settings (see Figure 3 for references and symbols). Solid and dashed curves show the variations of these elements as a function of Cr#, calculated using the partitioning models of Witt-Eickschen and O'Neill (2005) [15]: 800 °C and 2780 ppm Ni in olivine (KD model 1), 1000 °C and 2780 ppm Ni in olivine (KD model 2), 800 °C and 3749 ppm Ni in olivine (KD model 3) and 1000 °C and 3749 ppm Ni in olivine (KD model 4).

A similar approach was used to model the variations of Sc, Ga and V, assuming that the partitioning of these elements into spinel is mainly controlled by equilibrium with clinopyroxene. In this case, Sc variations were calculated from the Sc distribution coefficient, while Ga and V were calculated from the Ga-Cr and V-Cr distribution coefficients, respectively [15]. Calculated Sc contents showed a slight increase with increasing Cr#, reproducing the observed variations of the Xen group (Figure 5c). Based on this model, which also showed a significant temperature dependence on the partitioning between spinel and clinopyroxene, the observed Sc variations in the Xen group reflected equilibrium with clinopyroxene at temperatures between 800 °C and 1000 °C, in good agreement with the Ni and Co models. Moreover, Ga variations were well reproduced, showing a decrease in Ga contents with increasing Cr# (Figure 5d). In this case, however, temperature was predicted to have an insignificant effect on the partitioning. The large variation observed in the Xen group could therefore be related to variable bulk Ga variations of the source peridotite.

Calculated V contents slightly increased with increasing Cr# and temperature. However, even by assuming the highest V content of a coexisting clinopyroxene (157 ppm), calculated V contents were still too low to reproduce satisfactorily the observed variations in the Xen group (Figure 5e). Only using lower Cr^{cpx}/Cr^{sp} ratios (0.015–0.030) and the highest V contents in clinopyroxene (157 ppm) would an agreement with the observed data be produced. We suggest that such a discrepancy, rather than being related to a wrong assumption on Cr^{cpx}/Cr^{sp}, reflects the redox-sensitive behaviour of V, which can be present at different valence states at mantle conditions [50]. As a matter of fact, the models of Witt-Eickschen and O'Neill (2005) [15] reproduced the observed variations for Cr-spinels in peridotites from non-cratonic settings, which possibly equilibrated at redox conditions comparable to those of the peridotites used for their calibration, but different from those of cratonic mantle peridotites. We speculate that the higher V contents in the Xen group might be a consequence of the more reduced nature of cratonic spinel-peridotites (as low as 5 log units below the fayalite-magnetite-quartz oxygen buffer, FMQ-4.9 to FMQ + 1.5 [51]) compared to non-cratonic peridotites (FMQ-1.5 to FMQ + 0.5 [52]), which would increase the compatibility of V in spinel [50].

5.5. On the Partitioning of Some Trace Elements between Cr-Spinels and Kimberlitic Melts

We used some of the available experimental studies on partition coefficients between spinel and melt [53–57] to model the composition of the melt in equilibrium with our Chr spinels. We selected a limited number of elements (V, Mn, Co, Ni, Cu, Zn, Ga, Zn). The test was made only for kimberlites for which a representative number of spinels were analyzed, i.e., International'naya, Komsomolskaya and Mir pipes. For each element, a minimum and a maximum value of the partition coefficient were selected, considering experimental spinels with Mg# and Cr# as close as possible to our natural samples (0.43-0.63 and 0.47-0.92, respectively). If more than one set of experiments were available with such spinels, then we selected the set with melts with compositions as close as possible to kimberlites (i.e., low-silica and alkali- and/or carbonate-rich; see Table 1).

Table 1. List of partition coefficients selected, relative source and composition of melts considered in the experiments.

Element	$D^{sp/melt}$	Source	Melt
V	1.62	[53]	Alkali basalt
	3.22	[55]	Picrite
Mn	0.70	[57]	CMAS
	0.90	[36]	FCMAST
Co	2.00	[55]	Ankaramite
	6.00	[53]	Alkali basalt
Ni	0.24	[55]	Ankaramite

	12.86	[55]	Ankaramite
Cu	0.20	[57]	Komatiite
	0.80	[57]	MORB
Zn	1.00	[53]	Alkali basalt
	12.00	[58]	CMAST
Ga	3.10	[53]	Alkali basalt
	11.30	[36]	FCMAST
Zr	0.02	[36]	FCMAST
	0.14	[53]	Alkali basalt

Figure 6 shows the results of the model normalised to Primitive Mantle (PM [38]) and the comparisons with the compositions of the kimberlite hosts [23,34]. Calculated values for Cu, Ga and Zr were generally comparable to the composition of the kimberlites. Manganese and Ni were in the range of kimberlites only if the minimum $D_x^{(sp/melt)}$ was considered (see Table1) and only in International'naya and Mir pipes. It is worth noting that Wijbrans et al. (2015) [36] underlined how Mn appears as independent from temperature and oxygen fugacity but may be sensitive to the composition of spinel, with $D_{Mn}^{(sp/melt)}$ higher in Fe^{2+}-rich spinels compared to Mg-rich ones. Even $D_{Ni}^{(sp/melt)}$ values are independent from temperature and $f0_2$, but the partition coefficient seems to be higher in Ti- and Fe^{3+}- bearing spinels [55].

Cobalt and Zn showed values comparable to the kimberlite only for Mir pipe and only when considering the higher partition coefficient (see Table 1).

Vanadium was the only element always higher than the kimberlite values, which may be related to the sensitivity of this element to oxygen fugacity [36,53] or to the combination of this variable with temperature and spinel chemistry [55].

There are two main possible sources for discrepancies between real kimberlites and the modelled ones: (i) the measured composition of the host kimberlites did not represent the melt from which the Chr chromites crystallised, either because the analyses were contaminated by the presence of lithic fragments and secondary alterations or because the deep-seated proto-kimberlitic melts had substantially different compositions with respect to the erupted kimberlite; (ii) the partition coefficients for Cr-spinels in equilibrium with proto-kimberlitic melts were higher (or lower, depending on the case) than the values obtained by the various authors in the literature (see Table 1).

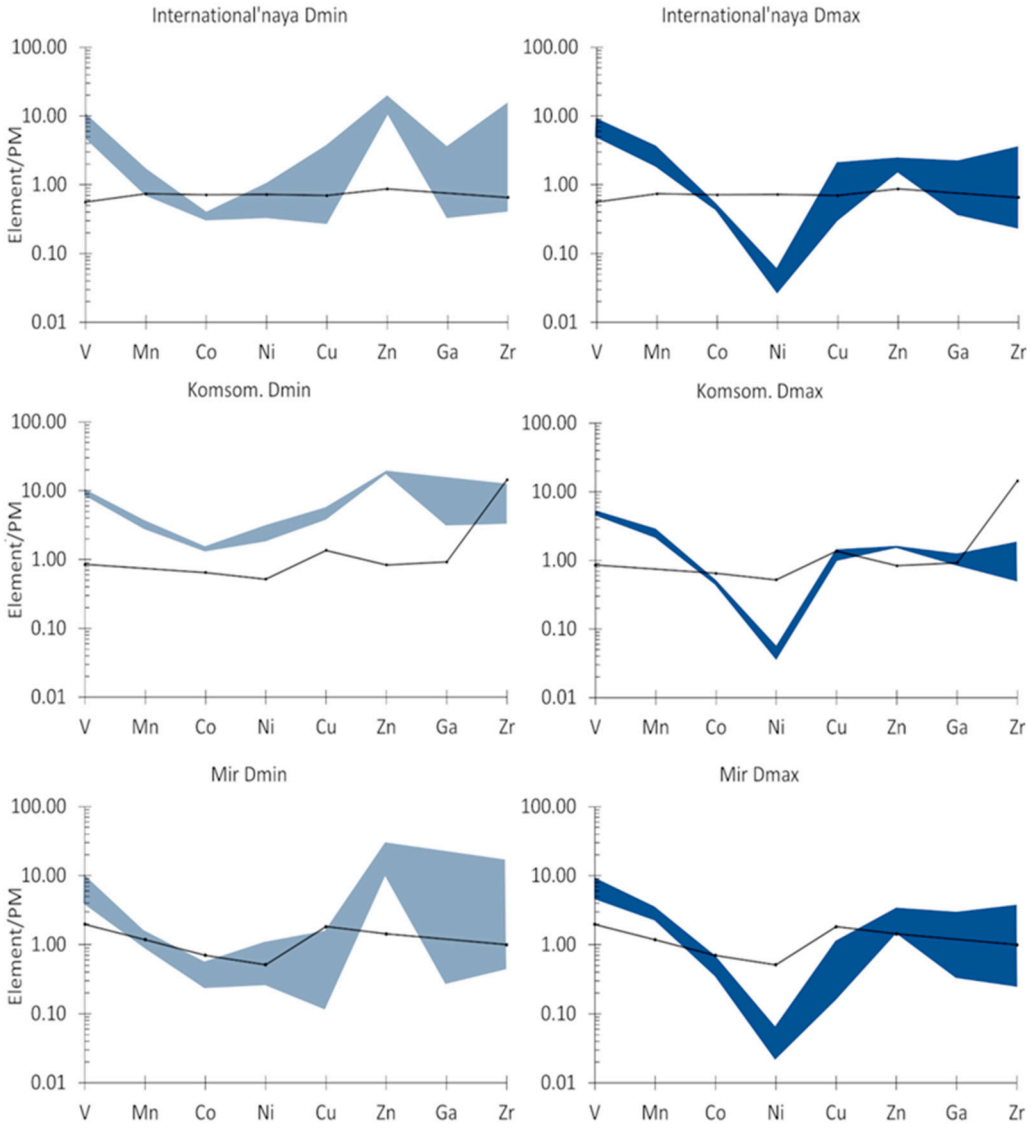

Figure 6. Modelled melts in equilibrium with Chr spinels. Light and dark blue spidergrams show the modelled melt compositions obtained with the minimum and maximum $D^{sp/melt}$, respectively (see Table 1). Black lines represent the kimberlite whole rock compositions from [34]. Data normalised to Primitive Mantle from [38].

6. Conclusions

This work gives new information on the spinel trace element budget in cratonic peridotites and kimberlites. Considering that Cr-spinels could be the sole surviving primary mineral in a matrix of altered silicates from ultramafic rocks, the different concentrations of certain elements could be important in distinguishing Cr-spinels from peridotites and crystallised from a kimberlitic melt. This could be extremely important in prospecting and paleogeographic reconstructions.

Comparing our data with the trace element contents of spinel included in diamond would be an efficient way to better constrain the environment where spinel and diamonds are formed and the possible trace element exchanges within minerals present at the same pressure and temperature in such important georesources as kimberlites are.

We combined our data to the partitioning models of Witt-Eickschen and O'Neill (2005) [15], simulating the composition of hypothetical spinels equilibrated in peridotitic assemblage, and found that our samples were in agreement with the model only for some

trace elements and preferentially for Xen spinels, as expected considering the source of this crystals.

Finally, we selected from the literature some of the partition coefficients experimentally determined to model the composition of a melt in equilibrium with our Chr spinels. The results showed a partial overlap with the real kimberlite values but only for few elements (mainly Cu, Ga and Zr), whereas others, such as V for example, were never close to the kimberlite composition. This simulation highlighted that we need more experimental data on trace elements $D_x^{(sp/melt)}$ for silicate–carbonate melts and particularly for spinels from kimberlites and related rocks.

Supplementary Materials: The following supporting information can be downloaded at: https://www.mdpi.com/article/10.3390/min12111439/s1, Figure S1: Co vs. Zn diagram for the Cr-spinels from this study and from peridotite xenoliths of continental setting; Supplementary Data S1: analytical data.

Author Contributions: Conceptualization, M.V. and D.L.; formal analysis, M.V., M.P., V.L. and G.T.; writing—original draft preparation, M.V., L.Z., F.P., A.L., N.V.S. and D.L.; writing—review and editing, M.V. All authors have read and agreed to the published version of the manuscript.

Funding: This research received no external funding.

Acknowledgments: D.L. would like to thank FRA2009 funds from Trieste University. Lorenzo Furlan at Trieste University for assistance in mount preparation and Andrea Risplendente at Milan University for assistance in microprobe analyses are kindly acknowledged.

Conflicts of Interest: The authors declare no conflict of interest.

References

1. Irvine, T.N. Chromian spinel as a petrogenetic indicator. Part 1. Theory. *Can. J. Earth Sci.* **1965**, *2*, 648–672.
2. Barnes, S.J.; Roeder, P.L. The Range of Spinel Compositions in Terrestrial Mafic and Ultramafic Rocks. *J. Petrol.* **2001**, *42*, 2279–2302.
3. Sobolev, N.V.; Logvinova, A.M. Significance of Accessory Chrome Spinel in Identifying Serpentinite Paragenesis. *Int. Geol. Rev.* **2005**, *47*, 58–64.
4. Griffin, W.L.; Ryan, C.G.; Gurney, J.J.; Sobolev, N.V.; Win, T.T. Chromite macrocrysts in kimberlites and lamproites: Geochemistry and origin. In Proceedings of the 5th International Kimberlite Conference, Minas Gerais, Brazil, 1994; pp. 366–377.
5. Lenaz, D.; Kamenetsky, V.S.; Crawford, A.J.; Princivalle, F. Melt inclusions in detrital spinel from the SE Alps Italy±Slovenia): A new approach to provenance studies of sedimentary basins. *Contrib. Mineral. Petrol.* **2000**, *139*, 748–758.
6. Kamenetsky, V.; Crawford, A.J.; Meffre, S. Factors controlling chemistry of magmatic spinel: An empirical study of associated olivine, Cr-spinel and melt inclusion from primitive rocks. *J. Petrol.* **2001**, *42*, 655–671.
7. Schulze, D.J. Origins of chromian and aluminous spinel macrocrysts from kimberlites in southern Africa. *Can. Mineral.* **2001**, *39*, 361–376.
8. Sobolev, N.V.; Logvinova, A.M.; Zedgenizov, D.A.; Seryotkin, Y.V.; Yefimova, E.S.; Floss, C.; Taylor, L.A. Mineral inclusions in microdiamonds and macrodiamonds from kimberlites in Yacutia: A comparative study. *Lithos* **2004**, *77*, 225–242.
9. Melcher, F.; Grum, W.; Simon, G.; Thalhammer, T.V.; Stumpfl, E.F. Petrogenesis of the Ophiolitic Giant Chromite Deposits of Kempirsai, Kazakhstan: A study of solid and fluid inclusions in chromite. *J. Petrol.* **1997**, *38*, 1419–1458.
10. Ahmed, A.H.; Arai, S.; Abdel-Aziz, Y.M.; Rahimi, A. Spinel composition as a petrogenetic indicator of the mantle section in the Neoproterozoic Bou Azzer ophiolite, Anti-Atlas, Morocco. *Precambrian Res.* **2005**, *138*, 225–234.
11. Ziberna, L.; Nimis, P.; Zanetti, A.; Marzoli, A.; Sobolev, N.V. Metasomatic processes in the Central Siberian Cratonic mantle: Evidence from garnet xenocrysts from the Zagadochnaya kimberlite. *J. Petrol.* **2013**, *54*, 2379–2409.
12. Ashchepkov, I.V.; Kuligin, S.S.; Vladykin, N.V.; Downes, H.; Vavilov, M.A.; Nigmatulina, E.N.; Babushkina, S.A.; Tychkov, N.S.; Khemelnikova, O.S. Comparison of mantle litosphere beneath early Triassic kimberlite fields in Siberian craton reconstructed from deep-seated xenocrysts. *Geosci. Front.* **2016**, *7*, 639–662.
13. Griffin, W.L.; Sobolev, N.V.; Ryan, C.G.; Pokhilenko, N.P.; Win, T.T.; Yefimova, E.S. Trace elements in garnets and chromites: Diamond formation in the Siberian lithosphere. *Lithos* **1993**, *29*, 235–256.
14. Paktunc, A.D.; Cabri, L.J. A proton-and electron-microprobe study of gallium, nickel and zinc distribution in chromian spinel. *Lithos* **1995**, *35*, 261–282.
15. Witt-Eickschen, G.' O'Neill, H.S.C. The effect of temperature on the equilibrium distribution of trace elements between clinopyroxene, orthopyroxene, olivine and spinel in upper mantle peridotite. *Chem. Geol.* **2005**, *221*, 65–101.
16. Norman, M.D. Melting and metasomatism in the continental lithosphere: Laser ablation ICPMS analysis of minerals in spinel lherzolites from eastern Australia. *Contrib. Mineral. Petrol.* **1998**, *130*, 240–255.

17. Glaser, S.M.; Foley, S.F.; Günther, D. Trace element compositions of minerals in garnet and spinel periodotite xenoliths from the Vitim volcanic field, Transbaikalia, eastern Siberia. In *Developments in Geotectonics*; Elsevier: Amsterdam, The Netherlands, 1999; Volume 24, pp. 263–285.
18. Lenaz, D.; Musco, M.E.; Petrelli, M.; Caldeira, R.; De Min, A.; Marzoli, A.; Mata, J.; Perugini, D.; Princivalle, F.; Boumehdi, M.A.; et, al. Restitic or not? Insight from trace element content and crystal—Structure of spinels in African mantle xenoliths. *Lithos* **2017**, *278*, 464–476.
19. Aulbach, S.; Giuliani, A.; Fiorentini, M.L.; Baumgartner, R.J.; Savard, D.; Kamenetsky, V.S.; Caruso, S.; Danyushevky, L.V.; Powell, W.; Griffin, W.L. Siderophile and chalcophile elements in spinels, sulphides and native Ni in strongly metasomatised xenoliths from the Bultfontein kimberlite (South Africa). *Lithos* **2021**, *380*, 105880.
20. Cherepanova, Y.; Artemieva, I.M.; Thybo, H.; Chemia, Z. Crustal structure of the Siberian craton and the West Siberian basin: An appraisal of existing seismic data. *Tectonophysics* **2013**, *609*, 154–183.
21. Davis, G.L.; Sobolev, N.V.; Kharkiv, A.D. New data on the age of Yakutian kimberlites obtained by the uranium-lead method on zircons. *Dokl. Akad. Nauk SSSR* **1980**, *254*, 175–179.
22. Griffin, W.L.; Ryan, C.G.; Kaminsky, F.V.; O'Reilly, S.Y.; Natapov, L.M.; Win, T.T.; Kinny, P.D.; Ilupin, I.P. The Siberian lithosphere traverse: Mantle terranes and the assembly of the Siberian Craton. *Tectonophysics* **1999**, *310*, 1–35.
23. Kostrovitsky, S.I.; Morikiyo, T.; Serov, I.V.; Yakovlev, D.A.; Amirzhanov, A.A. Isotope-geochemical systematics of kimberlites and related rocks from the Siberian Platform. *Russ. Geol. Geophys.* **2007**, *48*, 272–290.
24. Pearce, J.G.; Perkins, W.T.; Westgate, J.A.; Gorton, M.P.; Jackson, S.E.; Neal, C.R.; Chenery, S.P. A compilation of new and published major and trace element data for NIST SRM 610 and NIST SRM 612 glass reference materials. *Geostand. Newslett.* **1997**, *21*, 115–144.
25. Lenaz, D.; Logvinova, A.M.; Princivalle, F.; Sobolev, N.V. Structural parameters of chromite included in diamond and kimberlites from Siberia: A new tool for discriminating ultramafic source. *Am. Mineral.* **2009**, *94*, 1067–1070.
26. Lenaz, D.; Skogby, H.; Logvinova, A.M.; Sobolev, N.V.; Princivalle, F. A micro-Mössbauer study of chromites included in diamond and other mantle-related rocks. *Phys. Chem. Miner.* **2013**, *40*, 671–679.
27. Droop, G.T. A general equation for estimating Fe^{3+} concentrations in ferromagnesian silicates and oxides from microprobe analyses, using stoichiometric criteria. *Mineral. Mag.* **1987**, *51*, 431–435.
28. Abersteiner, A.; Giuliani, A.; Kamenetsky, V.S.; Phillips, D. Petrographic and melt-inclusion constraints on the petrogenesis of a magmaclast from the Venetia kimberlite cluster, South Africa. *Chem. Geol.* **2017**, *455*, 331–341.
29. Kumar, S.P.; Shaikh, A.M.; Patel, S.C.; Sheikh, J.M.; Behera, D.; Pruseth, K.L.; Ravi, S.; Tappe, S. Multi-stage magmatic history of olivine–leucite lamproite dykes from Banganapalle, Dharwar craton, India: Evidence from compositional zoning of spinel. *Mineral. Petrol.* **2021**, *115*, 87–112.
30. Roeder, P.L.; Schulze, D.J. Cristallization of groundmass spinel in kimberlite. *J. Petrol.* **2008**, *49*, 1473–1495.
31. Doucet, L.S.; Ionov, D.A.; Golovin, A.V.; Pokhilenko, N.P. Depth, degrees and tectonic settings of mantle melting during craton formation: Inferences from major and trace element compositions of spinel harzburgite xenoliths from the Udachnaya kimberlite, central Siberia. *Earth Planet. Sci. Lett.* **2012**, *359*, 206–218.
32. Grégoire, M.; Tinguely, C.; Bell, D.R.; Le Roex, A.P. Spinel lherzolite xenoliths from the Premier kimberlite (Kaapvaal craton, South Africa): Nature and evolution of the shallow upper mantle beneath the Bushveld complex. *Lithos* **2005**, *84*, 185–205.
33. Kopylova, M.G.; Russell, J.K.; Cookenboo, H. Petrology of peridotite and pyroxenite xenoliths from the Jericho kimberlite: Implications for the thermal state of the mantle beneath the Slave craton, northern Canada. *J. Petrol.* **1999**, *40*, 79–104.
34. Kostrovitsky, S.; Spetsius, Z.; Yakovlev, D.; Fon der Flaass, G.; Bogush, I.; Pokhilenko, N. *Atlas of the Igneous Rocks and Diamond Deposits of the Yakut Kimberlite Province*; Pokhilenko, N., Ed.; "MPG": Mirniy, Russia, 2015; p. 480.
35. Navrotsky, A.; Kleppa, O.J. The thermodynamics of cation distributions in simple spinels. *J. Inorg. Nucl. Chem.* **1967**, *29*, 2701–2714.
36. Wijbrans, C.H.; Klemme, S.; Berndt, J.; Vollmer, C. Experimental determination of trace element partition coefficients between spinel and silicate melt: The influence of chemical composition and oxygen fugacity. *Contrib. Mineral. Petrol.* **2015**, *169*, 45.
37. Griffin, W.L.; Ryan, C.G. Trace elements in indicator minerals: Area selection and target evaluation in diamond exploration. *J. Geochem. Explor.* **1995**, *53*, 311–337.
38. McDonough, W.F.; Sun, S.S. The composition of the Earth. *Chem. Geol.* **1995**, *120*, 223–253.
39. Shannon, R.D. Revised effective ionic radii and systematic studies of interatomic distances in halides and chalcogenides. *Acta Crystallogr. (A)* **1976**, *32*, 751–767.
40. O'Neill, H.S.C.; Navrotsky, A. Simple spinels: Crystallographic parameters, cation radii, lattice energies and cation distributions. *Am. Mineral.* **1983**, *68*, 191–194.
41. Lavina, B.; Salviulo, G.; Della Giusta, A. Cation distribution and structure modelling of spinel solid solutions. *Phys. Chem. Miner.* **2002**, *29*, 10–18.
42. Derbyshire, E.J.; O'Driscoll, B.; Lenaz, D.; Gertisser, R.; Kronz, A. Compositionally heterogeneous podiform chromitite in the Shetland Ophiolite Complex (Scotland): Implications for chromitite petrogenesis and late-stage alteration in the upper mantle portion of a supra-subduction zone ophiolite. *Lithos* **2013**, *162–163*, 279–300. https://doi.org/10.1016/j.lithos.2012.11.013.
43. Derbyshire, E.J.; O'Driscoll, B.; Lenaz, D.; Zanetti, A.; Gertisser, R. Chromitite petrogenesis in the mantle section of the Ballantrae Ophiolite Complex (Scotland). *Lithos* **2019**, *344–345*, 51–67.

44. Colás, V.; Padròn-Navarta, J.A.; González-Jiménez, J.M.; Griffin, W.L.; Fanlo, I.; O'Reilly, S.Y.; Gervilla, F.; Proenza, J.A.; Pearson, N.J.; Escayola, M.P. Compositional effects of the solubility of minor and trace elements in oxide spinel minerals: Insight from crystal-crystal partition coefficient in chromite exsolution. *Am. Mineral.* **2016**, *101*, 1360–1372.
45. Burns, R.G. The partitioning of trace transition elements in crystal structures: A provocative review with applications to mantle geochemistry. *Geochem. Et Cosmochim. Acta* **1973**, *37*, 2395–2403.
46. Stosch, H.G. Sc, Cr, Co and Ni partitioning between minerals from spinel peridotite xenoliths. *Contrib. Mineral. Petrol.* **1981**, *78*, 166–174.
47. Bulanova, G.P.; Speich, L.; Smith, C.B.; Gaillou, E.; Kohn, S.C.; Wibberley, E.; Chapman, J.G.; Howell, D.; Davy, A.T. The Unique Nature of Argyle Fancy Diamonds: Internal Structure, Paragenesis, and Reasons for Color. In *Geoscience and Exploration of the Argyle, Bunder, Diavik, and Murowa Diamond Deposits*; 2018, Society of Economic Geologists, 20, USA.
48. Dare, S.A.; Pearce, J.A.; McDonald, I.; Styles, M.T. Tectonic discrimination of peridotites using fO2–Cr# and Ga–Ti–FeIII systematics in chrome–spinel. *Chem. Geol.* **2009**, *261*, 199–216.
49. Ionov, D.A.; Doucet, L.S.; Ashchepkov, I.V. Composition of the lithospheric mantle in the Siberian craton: New constraints from fresh peridotites in the Udachnaya-East kimberlite. *J. Petrol.* **2010**, *51*, 2177–2210.
50. Mallmann, G.; O'Neill, H.S.C. The crystal/melt partitioning of V during mantle melting as a function of oxygen fugacity compared with some other elements (Al, P, Ca, Sc, Ti, Cr, Fe, Ga, Y, Zr and Nb). *J. Petrol.* **2009**, *50*, 1765–1794.
51. Rielli, A.; Tomkins, A.G.; Nebel, O.; Brugger, J.; Etschmann, B.; Paterson, D. Garnet peridotites reveal spatial and temporal changes in the oxidation potential of subduction. *Sci. Rep.* **2018**, *8*, 16411.
52. Frost, D.J.; McCammon, C.A. The redox state of Earth's mantle. *Annu. Rev. Earth Planet. Sci.* **2008**, *36*, 389–420.
53. Horn, I.; Foley, S.F.; Jackson, S.E.; Jenner, G.A. Experimentally determined partitioning of high field strength-and selected transition elements between spinel and basaltic melt. *Chem. Geol.* **1994**, *117*, 193–218.
54. Sattari, P.; Brenan, J.M.; Horn, I.; McDonough, W.F. Experimental constraints on the sulfide-and chromite-silicate melt partitioning behavior of rhenium and platinum-group elements. *Econ. Geol.* **2002**, *97*, 385–398.
55. Righter, K.; Leeman, W.P.; Hervig, R.L. Partitioning of Ni, Co and V between spinel-structured oxides and silicate melts: Importance of spinel composition. *Chem. Geol.* **2006**, *227*, 1–25.
56. Brenan, J.M.; Finnigan, C.F.; McDonough, W.F.; Homolova, V. Experimental constraints on the partitioning of Ru, Rh, Ir, Pt and Pd between chromite and silicate melt: The importance of ferric iron. *Chem. Geol.* **2012**, *302*, 16–32.
57. Liu, L.; Ma, Y.; Yan, W.; Liu, X. Trace element partitioning between MgAl2O4-spinel and carbonatitic silicate melt from 3 to 6 GPa, with emphasis on the role of cation order-disorder. *Solid Earth Sci.* **2019**, *4*, 43–65.
58. Loroch, D.; Klemme, S.; Berndt, J.; Rohrbach, A. Experimentally determined trace element partition coefficients between hibonite, melilite, spinel, and silicate melts. *Data Brief* **2018**, *21*, 2447–2463.